Determining Cu–Speciation in the Cu–CHA Zeolite Catalyst: The Potential of Multivariate Curve Resolution Analysis of In Situ XAS Data

Determining Cu-speciation in the Cu-CHA zeolite catalyst: the potential of Multivariate Curve Resolution analysis of *in situ* XAS data

A. Martini[a], E. Alladio[a], E. Borfecchia[a,b]*

[a]*Department of Chemistry, NIS Centre and INSTM Reference Center, University of Turin, Via Giuria 7, Turin, 10125 Italy.*

[b]*Haldor Topsøe A/S, Haldor Topsøes Allé 1, Kgs. Lyngby, 2800 Denmark.*

Abstract

The Cu-CHA zeolite today represents an attractive platform to design catalysts for deNO_x applications by NH_3-assisted Selective Catalytic Reduction (NH_3-SCR) and for the low-temperature selective oxidation of methane to methanol (MTM). Accessing a quantitative understanding of Cu-speciation in this material is a key step to unveil structure-performance relationships for these high-impact processes. Herein, we select Cu-CHA as a case study to demonstrate the potential of chemometric approaches, such as Multivariate Curve Resolution (MCR) applied in combination with Principal Component Analysis (PCA). We employ these methods to assist the interpretation of X-ray Absorption Spectroscopy (XAS) experiments in the near-edge (XANES) region, determining the spectroscopic signatures and concentration profiles of the pure Cu-species formed. We pinpoint the composition impact on the material reducibility and highlight Cu-speciation-productivity relationships for the MTM process. Furthermore, we report novel insights on the formation of O_2-derived species in Cu-CHA, obtained from MCR analysis of High Energy Resolution Fluorescence Detected (HERFD) XANES data collected during thermal treatment of Cu-CHA in both He and O_2 gas flow. Multivariate analysis, in combination with the superior energy resolution adopted, allows us to identify an additional Cu(II) species. This component, different from the previously characterized Z[Cu(II)OH] moiety, is only formed at significant concentrations in O_2 and it is envisaged to play an important role in the MTM conversion.

Keywords

Cu-chabazite, zeolite-based catalyst, Multivariate Curve Resolution, Principal Component Analysis, XAS, HERFD-XANES, methane-to-methanol conversion

Introduction

In the last few years, the Cu-exchanged form of chabazite (Cu-CHA) has attracted a lot of attention due to its outstanding performance in NH_3-assisted selective catalytic reduction (NH_3-SCR) of NO_x gases [1-3]. Together with Cu-MFI [4,5] and Cu-MOR [6-9], Cu-CHA has been also recently proven as an attractive platform for the low-temperature selective partial oxidation of methane to methanol (MTM) [10-12], a *dream reaction* with enormous energetic and environmental implications [13,14].

The CHA framework is composed of double six-membered rings (6r), connected in an AABBCC sequence forming cavities with eight-membered rings windows (8r). Recently, thanks to the increasing number of studies focusing on this Cu-zeolite, it has become evident that the CHA topology, despite its simple structure, offers multiple docking sites for the Cu cations in both 6r and 8r [15,16,2,17-19].

From the recent literature, it clearly emerges that Cu location in the framework strongly depends on the sample composition in terms of Si/Al ratio and Cu loading [20-24]. In particular, two major Cu-sites in dehydrated Cu-CHA have been proposed. These include reduction-resistant $Z_2Cu(II)$ species (where Z_2 represents bonds to zeolite framework oxygens O_{fw} next to two neighbouring charge-balancing Al sites in framework T-sites) hosted in the 6r and redox-active Z[Cu(II)OH] complexes (where Z indicates bonds to O_{fw} next to an isolated Al atom in a framework T-site) preferentially stabilized in the 8r. Z[Cu(II)OH] species are known to undergo so-called 'self-reduction' [25,26] to ZCu(I) during thermal treatment in vacuum or in inert gas flow from ~ 200 °C upwards [18,23,24,27].

Recent studies in the MTM context have also shown that a number of framework-interacting O_2-derived Cu(II) species can be formed in Cu-zeolites after high temperature (typically 500 °C) activation in oxidant

atmosphere, possibly resulting either from the reaction of self-reduced ZCu(I) species with O_2 or from internal pathways involving redox-active Z[Cu(II)OH] complexes [27,28,6]. For Cu-CHA, these include monomeric Z[Cu(II)O_2^-] superoxides in different coordination geometries, as well as dinuclear Z[Cu(II)O_2Cu(II)]Z and Z[Cu(II)OCu(II)]Z Cu(II) moieties [27,28].

As an additional element of complexity, Cu-speciation in Cu-CHA is largely driven by the environmental conditions, such as the gas feed composition and temperature [29,30,23,31]. For instance, the most recent reports describe the dynamic formation of multinuclear Cu sites by NH_3-solvated Cu ions during low-temperature NH_3-SCR [32,33]. These works spectacularly exemplify how, in Cu-zeolites, temperature and chemical environment can be tuned either toward heterogeneous-like chemistry over Cu-sites docked to the zeolite framework, or towards cage-confined homogeneous-like chemistry over mobilized Cu-species.

In situ/*operando* X-ray absorption (XAS) and emission (XES) spectroscopy, often guided by DFT-assisted data modelling [34-37], are ideal techniques to shed light on the local structural and electronic properties of Cu-species formed during thermal activation and under reaction relevant conditions [35,38-41]. X-ray Absorption Near Edge Structure (XANES) is particularly sensitive to coordination geometry and oxidation state of the formed Cu species, with a variety of fingerprint peaks at the Cu K-edge [42,43]. Differently from what is observed in the Extended X-ray Absorption Fine Structure (EXAFS) region, XANES dependence on the data collection temperature can be safely neglected in most of the cases. The collection of High Energy Resolution Fluorescence Detected (HERFD) XANES using an undulator source and an X-ray spectrometer can further enhance the technique sensitivity, yielding the best possible signal-to-background ratio because the energy resolution is of the order of the core-hole lifetime broadening [40,41].

However, dealing with an element selective (probing *only* the Cu species in the system) but averaging technique (probing *all* the Cu species in the system), the resulting spectral datasets in most of the cases consist in a mixture of different components related to the individual, 'pure' Cu-species, occurring with composition- and conditions-dependent relative abundances. This often complicates the interpretation of the collected spectra and prevents an accurate quantitative determination of Cu-speciation in the sample, ultimately representing a key requirement to establish structure-activity relationships.

To overcome the above-mentioned problem, a factorial procedure called Multivariate Curve Resolution (MCR) can be applied, in combination with Principal Component Analysis (PCA). This approach allows decomposing the original spectral dataset into chemically/physically meaning spectra and their own concentration profiles [44-48]. The method was initially introduced by Tauler and *al.* [45] and largely used during the last two decades in different fields of research, ranging from chromatography to image analysis [49,48]. Despite its usefulness, the application of this method to XAS data remains still rather limited. Nonetheless, in the last years, an increasing numbers of research groups have begun to use it in the analysis of large XAS datasets on different topics, such as battery research [50], quantum-confined systems [51], solid-state chemistry [52] and heterogeneous catalysis [53-56].

The MCR approach is especially useful and powerful when 'big' dataset (with typical size in the order of 100 scans or larger) are simultaneously analysed: this is becoming more and more the case for *operando* XAS studies in catalysis. Today, thanks to the continuous instrumental developments at synchrotron sources, efficient data collection at relatively short time-resolution (indicatively from few minutes on conventional XAS beamlines, down to few ms using dispersive setups [57] for Cu-zeolites samples with Cu-loading in the 2−4 wt % range) can be achieved under reaction-relevant conditions.

Herein we will highlight the potential of the MCR method to accurately determine Cu-speciation in Cu-CHA catalysts, summarising the recent results obtained by our group. We will then report novel insights derived from PCA and multi-way MCR analysis of HERFD-XANES data collected during thermal treatment in both inert and O_2 flow on a representative Cu-CHA sample (Cu/Al = 0.5; Si/Al = 12), discussing in detail the adopted procedure and providing a critical overview on the point of strength and limitations of the method.

Experimental

Details on Multivariate Curve Resolution Alternating Least Squares (MCR-ALS) analysis

General description of the MCR-ALS algorithm

The MCR procedure describes the original dataset **D**, constituted of q spectra, as the product of a **S** matrix, composed by $N < q$ complete set of pure spectra and a matrix **C** which elements correspond to signal-related concentration profiles. The original dataset is thus described by the following equation: $\mathbf{D} = \mathbf{C}\,\mathbf{S}^T + \mathbf{E}$, where $\mathbf{S}^T$ is the transpose of matrix **S**, while **E** represents the error matrix associated to the reconstruction.

In order to realize this kind of bilinear decomposition, a specific algorithm called MCR-ALS is used. Basically, it performs the dissociation optimizing concentration profiles and pure spectra in an altering least square (ALS) under constraints [58,46,59]. The outstanding feature of this method is that MCR is able to isolate the sources of variation in a determinate data set without *a priori* assumption about the individual species contributions related to the global response [60]. For further details on the method, the interested reader is referred to refs. [58,49,48].

The first step of the algorithm requests the determination of the number of components that characterize the original data matrix. To this purpose, Principal Component Analysis (PCA) or Single Value Decomposition (SVD) are commonly performed [58,49,48].

Details on the implementation of MCR-ALS analysis in the present work

For MCR-ALS analysis we employed the Graphical User Interface (GUI) developed by Jaumot and co-workers [48], freely downloadable at http://www.mcrals.info/, using Matlab R2011b. The analysed dataset consisted in a column-wise augmented matrix obtained joining two data matrices composed by 53 HERFD-XANES spectra each (461 energy points per spectrum, in the 8975 − 9021 eV energy range), acquired during the temperature ramp from 37 to 500 °C, with a 5 °C/min heating rate in O_2 or He gas flow (data collection time ~ 2 min/spectrum).

The initial un-mixing data procedure was performed using the variable purity approach (*i.e.* SIMPLISMA algorithm) with an *allowed noise* parameter fixed at 5% [58]. The ALS routine run with determinate soft constraints: *non-negativity* for both pure spectra and concentration profiles (this constraint was carried out thanks to the fast non-negative least squares algorithm, *fnnl* [61]) and *closure* set to 1 applied to concentration profiles. In particular, this last condition can be seen as the expression of the mass balance, that is valid in XAS spectroscopy being technique element-selective on all the Cu-species present in the X-ray-probed sample volume. The optimization routine successfully converged after 32 iterations, resulting in the final ALS quality control parameters shown in Table 1.

Table 1. Final quality control parameters extracted from MCR-ALS algorithm. The two different values of %LOF differ on the definition of the initial data matrix: the experimental data matrix for %LOF (Experiment) and the PCA reconstructed data matrix in case of %LOF (PCA).

Quality control Parameters	Values
%LOF (Experiment)	0.823
%LOF (PCA)	0.264
Percent of variance explained R^2	99.993

Sample synthesis and compositional analysis

The CHA zeolite with Si/Al ~ 12 characterized in this work was prepared following the procedure reported in a previous study [3], by modulating the composition of the synthesis gel to achieve the desired Si/Al ratio in the framework. To introduce Cu ions, the calcined CHA zeolites was suspended in a Cu(II) acetate solution, and stirred at room temperature (RT) for 24 h; the resulting copper-exchanged zeolite was recovered by

filtration and dried at 50 °C. The elemental composition of the sample was evaluated by Energy Dispersive X-Ray Spectroscopy (EDS), resulting in Si/Al = 12.1; Cu/Al = 0.49, Cu concentration = 620 μmol/g (3.8 wt%).

In situ HERFD-XANES spectra acquisition and data reduction procedures

High Energy Resolution Fluorescence Detected (HERFD) XANES spectra reported in Figure 3 were acquired at the ID26 beamline of The European Synchrotron (ESRF, Grenoble, France). Each spectrum was acquired in fluorescence mode, detecting only photons whose energy corresponded to the maximum intensity of the Cu $K_{\beta 1,3}$ emission line (~8906 eV). This energy selection was performed using the (800) reflection of a Ge (100) analyser crystal set up in vertical Rowland geometry. The crystal was spherically bent following the Johann scheme to focus the fluorescence radiation onto an APD detector. For the incident beam a flat double-crystal Si (311) monochromator was employed. The time acquisition for each spectrum was set to 2 min. The measurements were conducted using a well-established gas-flow setup, based on the Microtomo reactor cell (developed by the ESRF Sample Environment team) [62], that allowed to precisely control the gas composition and the temperature inside, as described in details in our previous works [29,18]. The Cu-CHA sample was prepared in the form of a self-supporting wafer (ca. 100 mg of sample) and fixed inside the reactor cell. *In situ* XAS experiments during He and O_2 activation were performed heating the samples from 37 °C to 500 °C with a heating ramp of 5 °C/min and flowing in the Microtomo reactor cell 100 ml/min gas He or O_2, depending on the type of activation. All the collected HERFD-XANES spectra were normalized to unity edge jump using the Athena software from the Demeter package [63].

For preparation protocols and experimental details regarding the samples and the conventional transmission-mode XANES data used to derive the results reported in Figure 1 and Figure 2, the reader is referred to the Supporting Information of the original publications, refs. [24] and [27], respectively.

Results and discussions.

Composition-driven Cu-speciation and reducibility in He-activated Cu-CHA from MCR-ALS analysis

In our previous work [24], we applied the MCR procedure to Cu K-edge XANES spectra of series of six Cu-CHA samples, synthesized by systematically tuning their composition (Si/Al and Cu/Al ratios in the $\sim 5-29$ and $\sim 0.1-0.6$ range, respectively). The Cu-CHA samples were characterized by *in situ* XANES during the activation procedure in He, from 25 to 400 °C, to achieve a better spectroscopic contrast between reducible and not reducible Cu-sites and gain deeper insights in the self-reduction process in Cu-zeolites. After PCA of the temperature-dependent multi-composition XANES dataset (globally 72 scans), MCR-ALS analysis allowed us to single out the XAS signatures of the five pure Cu-species formed in the CHA cages during thermal treatment in inert gas flow.

These results are summarized in Figure 1. The theoretical XANES spectra obtained from MCR-ALS (Figure 1a) showed an excellent agreement with previous XAS studies on Cu-CHA [29,18] and the recent report by Paolucci *et al.* [23]. Based on the spectroscopic fingerprints of each theoretical XANES and the correspondent temperature-dependent concentration profiles, we were able to reliably assign each pure spectrum to the Cu-species shown in Figure 1b. The concentration profiles for the most representative compositional points (top panel: Cu/Al = 0.1, Si/Al = 5; middle panel: Cu/Al = 0.5, Si/Al = 15; bottom panel: Cu/Al = 0.6, Si/Al = 29) are reported in Figure 1c.

We found that at RT, Cu-speciation is largely dominated by mobile fully-hydrated Cu(II) ions (PC1: blue curve/bars in Figure 1), namely $[Cu(II)(H_2O)_n]^{2+}$ or $[Cu(II)(H_2O)_{n-1}(OH)^-]^+$ with $n = 6$. For all the investigated compositional points, the appearance of fully-dehydrated, framework-interacting Cu-sites is observed after the transient development of a Cu(II) 'dehydration intermediate' (PC5: green curve/bars in Figure 1). This species is most likely characterized by a four-coordinated pseudo square-planar structure, based on the similarity between the corresponding pure XANES spectrum and four-fold coordinated Cu(II) references, such as Cu(II)O and $[Cu(II)(NH_3)_4]^{2+}$.

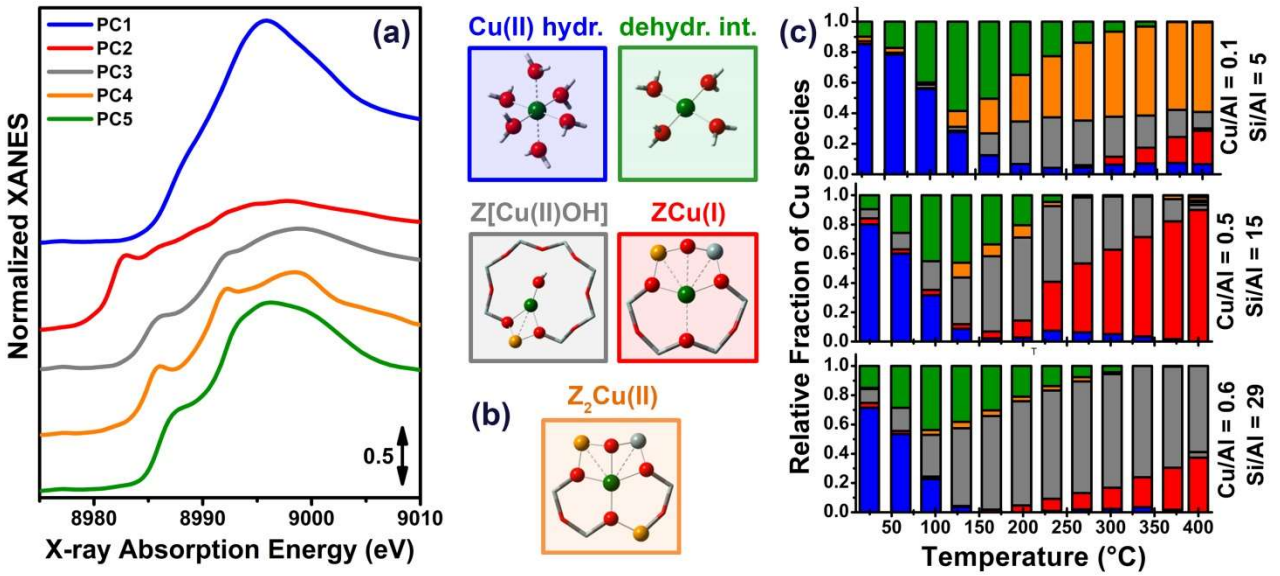

Figure 1. Results of MCR-ALS analysis of global temperature-dependent XANES dataset collected on six Cu-CHA samples with different composition during He-activation from 25 to 400 °C. (a) XANES spectra of pure components derived from MCR-ALS. Spectra have been vertically translated for the sake of clarity. (b) Proposed assignment of the five pure components to specific Cu-species/sites formed in the Cu-CHA catalyst as a function of composition and activation temperature, using the same colour code as in parts (a). Atom colour code in the structures: Cu, green; H, white; O, red, Si, grey; Al, yellow. (c) Bar plots reporting temperature-dependent concentration profiles of pure species for the most representative compositional points. Unpublished Figure, reporting data previously published in ref. [24].

At 400 °C, the entire speciation can be described as a combination of three specific framework-interacting Cu-species, occurring with composition-dependent relative abundance. The first one is represented by ZCu(I) sites (PC2: red curve/bars in Figure 1). Its pure spectrum can be unambiguously assigned to a Cu(I) species, due to the absence of the quadrupole $1s \rightarrow 3d$ transition in the pre-edge region (which is instead present in all the other pure spectra), and by the presence of a high intensity peak at ca. 8983 eV, assigned to $1s \rightarrow 4p$ transitions in two- and three-fold coordinated Cu(I) centers. The other two pure spectra are associated to two specific Cu(II) species: redox-active Z[Cu(II)OH] (PC3: grey curve/bars in Figure 1), preferentially located in the 8r, and redox-inert $Z_2Cu(II)$ sites in 6r (PC4: orange curve/bars in Figure 1).

The concentration of Z[Cu(II)OH] peaks around 200 °C and therein starts to progressively decrease, in favour of reduced ZCu(I) species. This is particularly evident for the Cu/Al = 0.5, Si/Al = 15 compositional point in Figure 1c, where at 400 °C ca. 90% total Cu occurs as ZCu(I) self-reduced species. Conversely, $Z_2Cu(II)$ sites, dominant at Si/Al = 5, reach a steady population in the 200–300 °C range and remain stable until 400 °C (see e.g. Cu/Al = 0.1, Si/Al = 5 in Figure 1c). Remarkably, the MCR-ALS results indicate that the reducibility level of Z[Cu(II)OH] complexes depends on the Al distribution in the framework. Indeed, as it can be clearly observed for Cu/Al = 0.6, Si/Al = 29 in Figure 1c, at high Si/Al values, the efficiency of the self-reduction process for Z[Cu(II)OH] is significantly lowered with respect to the Si/Al = 15 case, and only ca. 35% of ZCu(I) is detected at 400 °C.

The assignment of pure XANES spectra to specific Cu-species/sites presented above has been independently validated by DFT-assisted multi-component EXAFS fits and XANES simulations, and corroborated by complementary FTIR experiments using N_2 as a probe molecule for ZCu(I) sites [24].

In recent years, several studies [64,65,3,66,67] employed Electron Paramagnetic Resonance (EPR) spectroscopy to identify the Cu-species formed in Cu-CHA as a function of catalyst composition, temperature, and chemical environment. EPR ensures a high sensitivity to low-concentration Cu(II) species, while diamagnetic Cu(I) species are inherently silent. The technique thus shows a specific complementarity to the

averaging information from XAS. For this reason, herein we briefly compare the results reported in Figure 1 with complementary EPR insights reported in the literature.

EPR confirms that, irrespectively of the composition, mobile Cu(II) aquo complexes (PC1 in Figure 1) represent the major component in as-prepared Cu-CHA at ambient conditions. The correspondent EPR spectra are dominated by an isotropic species showing spin Hamiltonian parameters very similar to the ones of $[Cu(II)(H_2O)_n]^{2+}$ with n = 5, 6 species found in aqueous solution, with unresolved hyperfine coupling [66]. Conversely, low-field hyperfine structure is reported to become evident from ~ 250 °C, during thermal treatment in both inert and oxidant atmosphere. As reported by Gao et al. [65] for a Cu/Al = 0.032, Si/Al = 6 Cu-CHA sample, at the intermediate temperature of 150 °C, the intensity for the high-field EPR feature decreases dramatically, and the low-field hyperfine structures are completely absent. The authors explain these observations by dipolar interactions between Cu(II) ions. Considering the very low Cu loading for the investigated sample, such dipolar interactions below 250 °C imply the presence of highly mobile Cu(II) species, in good agreement with the under-coordinated Cu(II) aquo complexes highlighted by our MCR XANES analysis (PC5 in Figure 1).

Mossin and co-workers explored in detail by EPR the different copper positions in dehydrated Cu-CHA [64,66,67]. The authors rationalized the corresponding hyperfine structure with two EPR-active tetragonal Cu(II) sites, assigned to $Z_2Cu(II)$ species in 6rs with Al-Si-Al and Al-Si-Si-Al linkages. Local structure and composition-dependent abundance trends for these EPR-active species are in good qualitative agreement with the redox-inert PC4 component in Figure 1, although the different measurement conditions complicate a direct quantitative comparison. Overall, XANES MCR analysis indicates a lower fraction of 2Al $Z_2Cu(II)$ sites with respect to EPR spin quantification at equivalent composition. The same research group also suggested monomeric Cu(II) species with an approximate trigonal coordination, such as the 1Al Z[Cu(II)OH] complexes (PC3 in Figure 1), to be EPR-silent due fast relaxation [64,66]. In this case, specific in situ EPR experiments (rehydration in the presence or absence of O_2 traces of samples previously dehydrated in He or 20% O_2/He at 250 °C) allowed the authors to indirectly quantify these species hosted at 1Al sites. From these studies, 1Al Cu species are reported to represent the major Cu component (50% total Cu) at Cu/Al = 0.46, Si/Al = 14, occurring in their oxidized Z[Cu(II)OH] or reduced form ZCu(I) after dehydration in O_2/He or He, respectively [64,66]. The presence of small (< 13%) populations of EPR-silent, reduction-resistant Cu_xO_y species or small Cu oxide clusters is also suggested at the same catalyst composition. As we discussed in our previous work [24], these additional Cu(II) species are expected to show a XANES quite similar to the one Z[Cu(II)OH], and could not be discriminated by MCR-ALS XANES analysis during He-activation.

The use of MCR pure spectra as references in XANES Linear Combination Fit (LCF) analysis: correlating reducibility and productivity for methane to methanol conversion over Cu-CHA

LCF analysis is a well-established and easy-to-use method for disentangling the different species contributing to a XANES spectrum. Briefly, a normalized experimental XANES spectrum, $\mu_i^{exp}(E)$, can be expressed as the linear combination (LC) of N reference XANES spectra $\mu_i^{ref}(E)$ for known Cu-species: $\mu^{exp}(E) = \sum_{i=1}^{N} w_i^{ref} \cdot \mu_i^{ref}(E)$, where w_i^{ref} indicate the weights of each reference spectrum in the LC (i.e. the fractional concentration of the corresponding Cu-species). The LCF approach simply consists in optimizing the weights w_i^{ref} for each reference to obtain the best agreement to the experimental spectrum.

This approach has seen a widespread application to evaluate Cu-speciation during *in situ/operando* XAS experiments on Cu-exchange zeolite catalysts [31,6]. However, a pre-requisite for the successful application of the LCF analysis is the availability of an appropriate set of reference spectra. With respect to Cu-zeolites, the direct applicability of LCF largely depends on the environmental conditions. As mentioned above, within specific temperature ranges and chemical environments, the Cu cations are mobilized, occurring as well-defined molecular complexes suspended into the zeolite cages. This is *e.g.* the case for the as-prepared materials in air at RT or for low-temperature NH_3-SCR conditions [29,23,31-33], when the cations are

efficiently solvated by H_2O or NH_3, respectively. In such conditions, solution-phase references can be safely used to evaluate Cu-speciation by XANES LCF analysis [31]. Conversely, when framework-interacting Cu-species are formed, obtaining a proper set of experimental references is not straightforward, due to the unusual coordination modes to the zeolite framework adopted by the cations.

As discussed above, in the latter case MCR-ALS analysis represents a valid support to resolve spectral complexity. However, to improve the reconstruction results, it is important to collect a large dataset. Moreover, the global dataset should include scans where each structural component is present in a suitably large concentration, indicatively > 30% total Cu. Importantly, once the MCR-ALS pure spectra are obtained from a dataset which satisfies these criteria, they can be employed to precisely evaluate Cu-speciation in different Cu-CHA samples/conditions by simple LCF analysis.

As an example, we have recently taken advantage of the MCR-ALS results summarized in Section 0 to quantify the reducibility in a different batch of Cu-CHA zeolites with equivalent Cu/Al ratio of ~ 0.5 and different Si/Al ratios of ~ 5, 15 and 29 after He-activation at 500 °C [27]. To this aim, we applied LCF analysis as described above, but using as $\mu_i^{ref}(E)$ the five MCR-ALS curves reported in Figure 1a instead of experimental reference spectra.

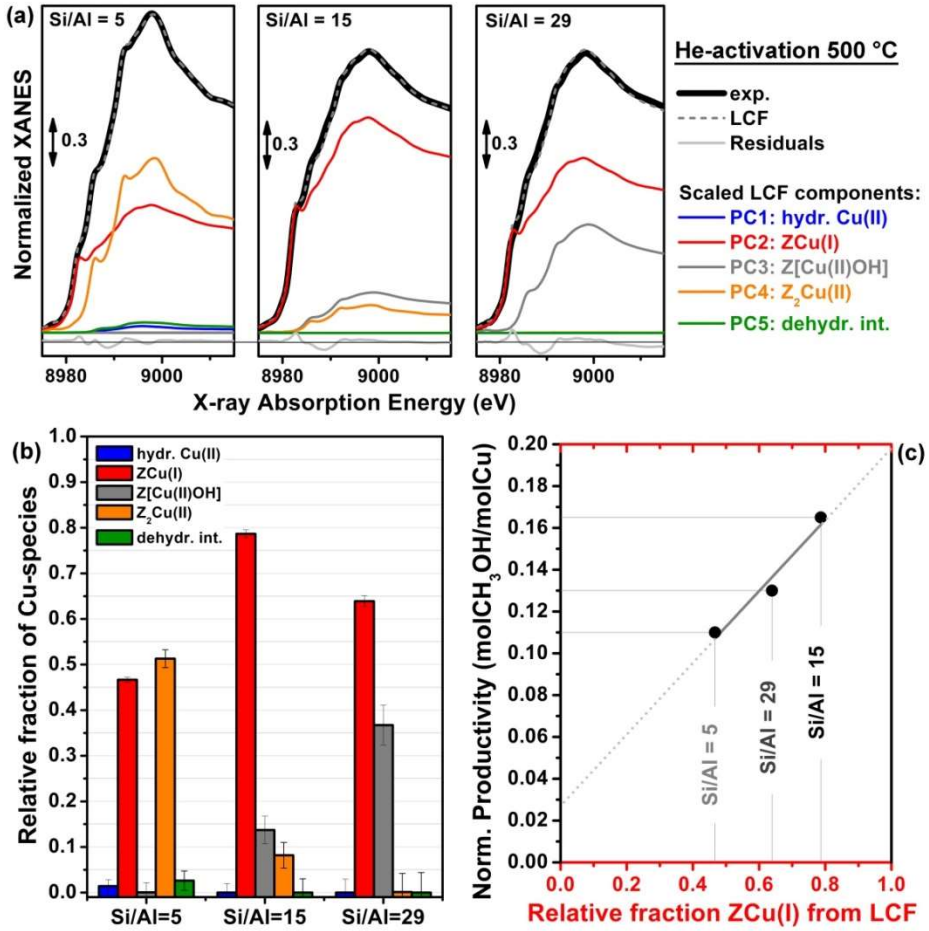

Figure 2. (a) Comparison between experimental XANES spectra of He-activated Cu-CHA samples with equivalent Cu/Al = 0.5 and Si/Al = 5 (left panel), 15 (middle panel), and 29 (right panel) with the correspondent best-fit curves from XANES LCF analysis using as reference the MCR-ALS spectra obtained in ref. [24] and reported in Figure 1a. For each fitted spectrum, the LCF components scaled by their respective optimized weights and the LCF residuals are reported. (b) Bar plot reporting the XANES LCF results for Cu-speciation in the He-activated state at 500 °C for the same samples reported in part (a). (c) Linear correlation between the productivity per Cu for the MTM process measured for the same Cu-CHA samples reported in part (a) and their reducibility in the He-activated state, quantified through the ZCu^I fraction obtained from XANES LCF analysis. Unpublished Figure, reporting results previously published in ref.[27].

The high LCF quality obtained using the theoretical XANES from MCR-ALS analysis can be noted in Figure 2a, which compares the experimental XANES for the three He-activated materials (black thick lines) with their correspondent best-fit curves (grey dashed lines): in all the cases, the fit R-factor was below 0.001. Such a high LCF quality is diagnostic for the presence of the same set of Cu-species, whose individual XANES signatures have been isolated using MCR-ALS in the previous work [24]. The Figure also reports the LCF scaled components, using the same colour code as in Figure 1, and the LCF residuals, as light grey thin lines.
The bar plot in Figure 2b provides an overview on the Cu-speciation from LCF analysis for the three investigated Cu-CHA samples. Not surprisingly, Cu-speciation in the He-activated state at 500 °C is dominated by framework-interacting Cu-species, including Cu-species hosted at *1Al* sites, in their oxidized, Z[Cu(II)OH], and self-reduced, ZCu(I), form as well as Z_2Cu(II) species, hosted at *2Al* sites in 6r. The contribution from mobile Cu(II) aquo-complexes, both fully and under coordinated, is < 3% total Cu for all the investigated samples. The composition-reducibility trends highlighted in Section 0 are confirmed here. Indeed, the Si/Al = 15 sample shows the highest reducibility (i.e. fraction of ZCu(I) species, being in this case (79 ± 1)% of total Cu). The reducibility is significantly lower at Si/Al = 5 (ZCu(I) species only account for (47 ± 1)% of total Cu), due to a large population of *2Al* Z_2Cu(II) sites. Also at Si/Al = 29 a lower fraction of ZCu(I) is detected, accounting for (64 ± 1)% of total Cu. Here, in line with the statistical scarcity of *2Al* docking sites in 6r at Si/Al = 29, the contribution of redox-inert Z_2Cu(II) species is negligible. However, the efficiency of the self-reduction process appears lowered with respect to the Si/Al = 15 case: (35 ± 4)% of total Cu is still present as oxidized Z[Cu(II)OH] species.
The same Cu-CHA samples characterized by XANES LCF analysis in their He-activated state at 500 °C were evaluated for the step-wise MTM process by laboratory fixed-bed reactor tests, as described in detail in ref. [27]. Correlating the LCF results reported in Figure 2b with the MTM performance of investigated Cu-CHA materials with equivalent Cu/Al = 0.5 and different Si/Al = 5, 15, 29, we observed a linear correlation between the normalized CH_3OH productivity and the sample reducibility in the He-activated state, quantified through the fraction of ZCu(I) from LCF analysis, as shown in Figure 2c.
Thus, the quantitative determination of Cu-speciation by XANES LCF analysis using MCR-ALS-derived references, allowed us to show how the reducibility in the He-activated state at 500 °C can be used as a descriptor for the methanol productivity in the MTM process over Cu-CHA. This correlation, together with many other lines of evidence, implies that: (i) *2Al* redox-inert Z_2Cu(II) sites are completely inactive for the MTM conversion; (ii) Z[Cu(II)OH] complexes at *1Al* sites are not directly active but are identified as the precursors to the active sites, possibly formed though Z[Cu(II)OH] self-reduction to ZCu(I) and subsequent reaction of ZCu(I) with O_2 to different Cu_xO_y active moieties.

Comparing He- and O_2-activation in Cu-CHA: preliminary results from MCR analysis of HERFD-XANES

As discussed in Section 0, the availability of redox-active Cu-species, efficiently undergoing self-reduction during thermal treatment, represents a crucial requirement for the MTM conversion over Cu-CHA. Although Z[Cu(II)OH] species are inactive by themselves, most likely they represent the precursors to different Cu(II) active sites, which formation requires high-temperature reaction with O_2. To obtain deeper insights in this point, herein we focus on a selected Cu-CHA sample (Si/Al = 12, Cu/Al = 0.5), resulting in an optimal performance for the MTM process (normalized productivity of 0.16 molCH_3OH/molCu with 87% selectivity, using optimized process conditions as described in details in ref. [27]). We applied MCR analysis on a combined HERFD-XANES dataset including both O_2- and He-activation for the selected material, in an attempt to single out the contribution from O_2-derived Cu-species.

HERFD-XANES during O_2- and He-activation: qualitative analysis

Figure 3 shows the two *in situ* HERFD-XANES datasets collected for the investigated Cu-CHA sample during activation in O_2 (Figure 3a) and in He (Figure 3b). From qualitative analysis, it is clear that the evolution of XANES features, during both activations, is consistent with thermally driven dehydration of the Cu centres:

the intensity of the white-line (W.L.) peak gradually decreases as the temperature increases, reflecting the progressive lowering in the average first-shell coordination number of Cu. In line with previous studies [18], the spectral evolution is rather insensitive to the gaseous environment up to ~ 250 °C. In both O_2 and He flow, the lowering in the W.L. intensity is accompanied by the development of a rising-edge shoulder around 8986 eV, which is imputable to the $1s \rightarrow 4p$ transition in four-fold or three-fold coordinated Cu(II) sites.
The use of HERFD-XANES instead of conventional one allows an optimal detection the weak pre-edge peak at 8977.5 eV (see Figure 3, insets) mostly arising from the $1s \rightarrow 3d$ transition in d^9 Cu(II) sites. The pre-edge peak is observed to slightly shift to higher energies and gain in its intensity as dehydration proceeds. Overall, the distinctive traits of the final spectrum at 500 °C in O_2 are in agreement with previous studies [29,17,68,24,18] indicating a largely dominant Cu(II) oxidation state. However, we observe that in the high-temperature range in O_2, certain modifications occur in the intensity and position of the Cu(II) $1s \rightarrow 4p$ rising-edge peak at 8986 eV, which could be connected with the presence of different dehydrated Cu(II) species.

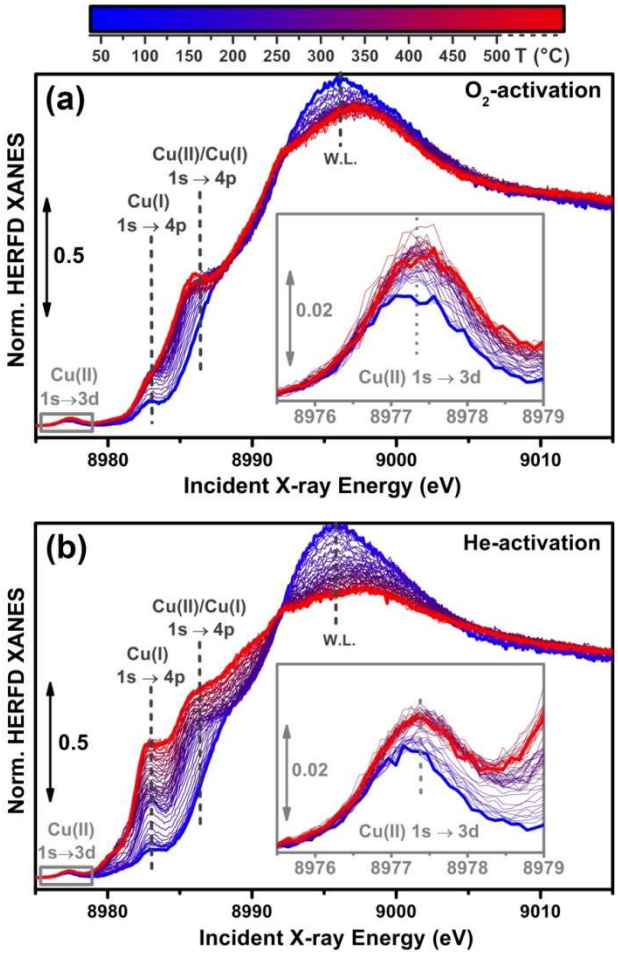

Figure 3. *In situ* temperature-dependent HERFD-XANES data collected at the ID26 beamline of the ESRF during (a) O_2-activation and (b) He-activation for Cu-CHA (Si/Al = 12, Cu/Al = 0.5). The top bar reports the colour code adopted to indicate the collection temperature for each scan, with the starting spectrum (37 °C) and ending spectrum (after ca. 10 min at 500 °C) reported as blue and red thick lines, respectively. The insets report a magnification of the $1s \rightarrow 3d$ Cu(II) pre-edge peak, highlighted by a grey box in the main panels; the energy positions for Cu(I) and Cu(II) $1s \rightarrow 4p$ rising-edge peaks and of the white-line peak (W.L.) are also indicated.

Regarding the activation in He, from ~ 250 °C upwards we observe the development of prominent rising-edge peaks from 8983 eV, as it is characteristic of ZCu(I) sites formed after self-reduction of redox-active Cu-species hosted at *1Al* sites [18,24,29]. The presence of a minor, but still significant, fraction of Cu(II) species in the He-activated sample is evidenced by the persistence of the pre-edge $1s \rightarrow 3d$ peak after ca. 15 min at

500 °C (see inset of Figure 3b, red thick curve). As anticipated, it can be better identified thanks to the improved energy resolution and lower signal-to-background ratio offered by HERFD-XANES. Similarly, we note the presence of a weak but well-defined peak in the characteristic Cu(I) $1s \rightarrow 4p$ energy region already at 37 °C, in both O_2 and He atmosphere. In O_2, this feature remains visible until 250 °C, while at higher temperature it is no more distinguishable from the tail of the rising-edge peak at 8986 eV. Conversely, in He, from 250 °C upwards, the 8983 eV peak it is observed to progressively develop in intensity, concomitantly with the formation of a large Cu(I) population *via* self-reduction.

In the following Section we will translate these qualitative insights into a quantitative evaluation of Cu speciation during the O_2- and He-activation processes, using chemometric approaches. Additional details on PCA analysis and results, as well as on the implementation of the MCR-ALS procedure with the support of experimental reference spectra can be found in the Supplementary Material.

MCR-ALS results: evidences for O_2-derived Cu(II) species

Figure 4 reports the MCR-ALS pure spectra for the 6 Principal Components (PCs) indicated by PCA (see Supplementary Material, Section 1), together their correspondent concentration profiles.

The pure HERFD-XANES spectra in Figure 4a show a substantial correspondence with the ones reported in Figure 1a, derived by applying MCR-ALS analysis to conventional transmission-mode XANES data on a compositionally larger dataset. Overall, beside specific limitations in the reconstruction which will be discussed below, the resulting MCR-ALS spectra could be safely attributed to physically-chemically meaningful contributions, involving the same set of Cu-species identified in the previous study summarized in Section 0 (namely PC1, PC2, PC3, PC5, PC6, assigned as indicated in Figure 4 to hydrated Cu(II), ZCu(I), Z_2Cu(II), Z[Cu(II)OH] and under-coordinated Cu(II) dehydration intermediate, respectively) plus an additional O_2-derived Cu(II) species, PC4 (yellow curve and bars).

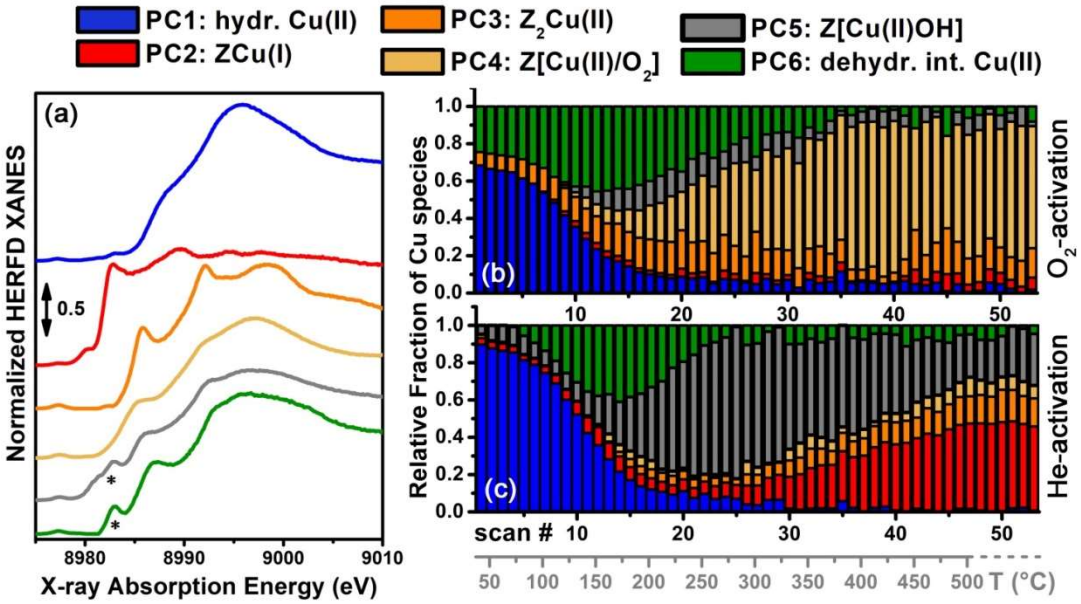

Figure 4. (a) Pure spectra isolated through combined 'multi-way' MCR-ALS analysis of the *in situ* HERFD-XANES data collected during O_2-activation and He-activation of a Cu-CHA samples with Cu/Al = 0.5; Si/Al = 12 (experimental data reported in Figure 3). Spectra have been vertically translated for the sake of clarity. The * symbol indicates the presence of reconstruction artefacts in the form of spurious rising-edge peaks for the spectra of PC5 and PC6. (b, c) Concentration profiles for the pure HERFD-XANES spectra reported in part (a) during (b) O_2-activation and (c) He-activation, plotted as a function of the scan number (2 min/scan, black axis and labels) and of the correspondent data collection temperature (grey axis and labels, from 37 °C to 500 °C, plus ~ 15 min dwelling time in isothermal conditions at 500 °C). For both parts (a) and (b), the same colour code is adopted to indicate the identified Cu-species, according to the legend reported in the top panel of the Figure; the colour code is the same as in Figure 1 for the five PCs present in both studies, namely PC1, PC2, PC3, PC5, PC6. PC4 (yellow curves and bars) is assigned to a novel O_2-derived Cu(II) species.

In the present case the reconstruction suffered of some limitations connected with the use of a one-composition dataset, which appeared to be enhanced due to higher energy resolution employed. In particular, some spurious peaks are observed in the energy range 8980 − 8984 eV (typical of Cu(I) $1s \rightarrow 4p$ transitions), in the MCR-ALS spectra for the last two components, PC5 and PC6 (denoted with * symbols in Figure 4a). As described in Section 0, a weak contribution in this range is observed experimentally already in the low-temperature range during both O_2 and He activation and could derive from traces of Cu(I) species other than ZCu(I), which could easily escape detection in conventional XANES due to their low concentration. Dealing with a very minor contribution, whose concentration profile is completely embedded in the concentration window of much more abundant Cu species, it was impossible to retrieve its spectral signature from MCR, and its most distinctive trait, *i.e.* the peak around 8982 eV, is fictitiously embedded into the PC5 and PC6 pure XANES spectra.
Further insights can be derived from the analysis of the concentration profiles in Figure 4b,c. Starting from the activation in He (Figure 4c), the trends in the Cu-speciation evolution are qualitatively consistent with the one reported in Figure 1c for the sample with Cu/Al=0.5 and Si/Al=15 [24]. The decreasing in the population of fully hydrated Cu(II) correlates with the appearance of the Cu(II) species previously described as a four-coordinated dehydration intermediate. At higher temperature, from ca. 170 °C upwards, Z[Cu(II)OH], progressively forms. Z[Cu(II)OH] concentration reaches a maximum of 80% at 200 °C and then progressively diminishes in the favour of ZCu(I). Z_2Cu(II) species appear from ~ 200 °C. Their concentration linearly growths with temperature until 400 °C, remaining then stable at ~ 15% total Cu during the final part of the heating ramp. The final state probed during He-activation, after 15 min in He at 500 °C, is characterized by a substantial fraction of reduced ZCu(I) sites, accounting for 51% of total Cu. The new Cu(II) species identified in this dataset, PC4, shows a very marginal role in the total signal representation. Its formation seems to be linked to the appearance of Z_2Cu(II) species, although its concentration during He-activation always remains below 7%.
During O_2-activation, MCR analysis evidences important differences in temperature-dependent Cu speciation with respect to the treatment in He. For the initial state, fully hydrated Cu(II) complexes are still the largely dominant structural component, but an important contribution from under-coordinated Cu(II) aquo-complexes (PC6) is already observed, representing 24% total Cu at 37 °C. Similarly, a minor population of Z_2Cu(II) sites (ca. 7%) is detected since the very beginning of the activation ramp. The concentration of these species undergoes a linear increase up to ca. 16%, reached at 170 °C. At higher temperature their abundance remains rather stable, although in the 400−500 °C range larger fluctuations are observed. Noteworthy, the final abundance of redox-inert Z_2Cu(II) species is poorly influenced by the activation atmosphere. It appears to be determined by the Si/Al ratio of the zeolite framework, which gives the statistical availability of docking sites in 6rs hosting two charge-balancing Al sites.
The most intriguing result is connected with the dynamics of Z[Cu(II)OH] and the new Cu(II) species (PC4) only detected in significant abundance in O_2 atmosphere. In particular, the two Cu(II) components seem to simultaneously develop from ca. 150 °C upwards, correlating with the diminution of the Cu(II) dehydration intermediate. Nonetheless, the Z[Cu(II)OH] species concentration remains rather low, oscillating around 13% until 400 °C, and further decreasing to below 10% at higher temperature. In parallel, the concentration of PC4 component progressively increases, becoming the dominant Cu component in the high-temperature range (70% total Cu at the end of the protocol). All along the O_2-activation, ZCu(I) always occurs only as a very minor species, with concentrations in the 2−5% ranges.
Comparing the behaviour of the PC4 component during thermal treatment under oxidant and inert conditions, it appears that this species is strongly associated with the availability of O_2 in the feed, whereas the Z[Cu(OH)] species is transiently present in large abundance also in He, before it undergoes self-reduction to ZCu(I). The XANES signatures of these two Cu(II) species are overall quite similar, indicating a similar Cu coordination geometry in the two cases. However, they do differ in the intensity and shape of the W.L. peak, being more intense for PC4 with a sharper maximum at 8997 eV, as well as in the energy position of the rising-edge peak,

red-shifted of 1 eV for PC4 with respect to PC5. With this respect, the use of HERFD-XANES it is crucial to discriminate the two structural components.
These results highlight how the PC space for O_2-activation has an higher dimensionality with respect to what found for He-activation (see also Supporting Material, Section 1). We associate the additional component with an O_2-derived Cu(II) species which could continuously originate from Z[Cu(OH)] precursor species, possibly though their transient reduction, on a timescale faster than time resolution employed here (2 min), and the re-oxidation of the newly formed Cu(I) species by O_2. Such process is in good agreement with the FTIR evidences reported by Pappas *et al.* [27], showing how the characteristic band at ~ 3650 cm^{-1}, assigned to the ν(OH) vibration in Z[Cu(OH)]species [69,18,23], decreases in intensity as temperature increase during O_2-activation in the RT-400 °C range.
The similarity of the MCR-ALS XANES spectra for PC4 with the one assigned to Z[Cu(OH)] suggests a similar three-fold coordinated Cu species, which most likely plays a crucial role in the MTM process. Possible candidates include monomeric Z[Cu(II)O_2^-] superoxo species with end-on coordination mode, as well as three-coordinated di-nuclear peroxo and oxo Cu(II) moieties, already identified in O_2-activated Cu-CHA from Raman spectroscopy [27,28]. Further studies will be needed to assess the exact chemical nature of the corresponding O_2-derived Cu(II) species, possibly in combination with DFT-assisted simulation of the XANES signatures for the different possible Cu_xO_y moieties indicated above.

Conclusions

In this work we have highlighted the potential of the MCR technique, applied in combination with PCA, to facilitate the interpretation of *in situ* XAS experiments aimed at the quantitative determination of Cu-speciation in Cu-CHA zeolites. These materials, intensively investigated in the context of high-impact processes such as NH_3-SCR and MTM conversion in mild conditions, have been selected as a representative example to demonstrate the general validity of the method in catalysis. Indeed, the CHA framework has been shown capable to host a rich variety of Cu species depending on compositional characteristic and chemical environment. These species often occur as a multi-component mixture, difficultly resolvable with the conventional data analysis approaches.
Focusing on Cu-CHA, we have provided an overview on MCR applications to identify pure Cu-species as a function of composition and to establish Cu-speciation-productivity relationships for the MTM process. In particular, MCR-ALS analysis on a large temperature/composition-dependent XANES dataset allowed singling out the XANES signatures of individual Cu-species formed and achieve unprecedented quantitative information on composition-induced effects on Cu-speciation and reducibility in Cu-CHA. The 'pure' XANES curves from MCR analysis have subsequently been employed to accurately determine Cu-speciation in a different series of He-activated Cu-CHA zeolites (Si/Al = 5, 15, 29; constant Cu/Al = 0.5) by simple LCF analysis. Correlating the LCF results with the performance of the investigated Cu-zeolites for the MTM process, we found a linear correlation between the normalized methanol productivity and the sample reducibility. These results indicated that high populations of Z_2Cu(II) sites in 6r, favoured at low Si/Al ratios, inhibit the material performance by being inactive for the MTM conversion. Z[Cu(II)OH] complexes, although shown to be inactive, are identified as the precursors to the methane-converting active sites.
These latter points, connected with the presence of specific O_2-derived Cu(II) species in Cu-CHA, has been deepened in the present work, by applying the MCR-ALS technique to the analysis of a 'multi-way' HERFD-XANES dataset including spectra collected during activation in both O_2 and He gas flow. With this respect, we underlined both the strengths and the weakness of the method, together with possible strategies to improve the quality of the reconstruction.
The use of PCA and MCR-ALS, in combination with the superior energy resolution of the HERFD-XANES technique, has allowed us to highlight an higher degree of complexity in Cu-speciation during O_2-activation with respect to the He-activation, which would have been difficult to appreciate using the conventional approaches in XAS data analysis. Data analysis revealed the presence of an additional Cu(II) species, different

from the previously characterized Z[Cu(II)OH] one. This component, only formed at significant concentrations in the case of O_2-activation, it is envisaged to play an important role in the MTM conversion. Overall, the reported results for Cu-CHA, evidence how synergizing the structural/chemical sensitivity of synchrotron-based X-ray spectroscopy with chemometric techniques can result in an enhanced quantitative understanding of conditions- and composition-dependent metal speciation in complex nano-catalysts.

Acknowledgements
EB acknowledges Innovation Fund Denmark (Industrial postdoc n. 5190-00018B). We are deeply indebted with many colleagues from different institutions working in the context of a fruitful and stimulating collaboration on Cu-zeolite catalysts, for insightful discussions and support on XAS data collection and analysis, chemometric techniques, chemistry and catalysis of the studied materials. In particular we thank C. Lamberti, S. Bordiga, G. Berlier, C. Negri, and M. Vincenti from University of Turin; I. A. Pankin from University of Rostov-on Don and University of Turin; P. Beato, H. Falsig, S. Teketel from Haldor Topsøe A/S; S. Svelle, D. K. Pappas, M. M. Dyballa from University of Oslo. A special acknowledgment goes to the staff of The European Synchrotron for the competent support during data collection on the BM23 (M. Monte Caballero) and ID26 beamlines (R. Baran); we also acknowledge K. A. Lomachenko (scientist at BM23/ID24) for the continuous scientific and technical support on the whole research project.

References

1. Beale AM, Gao F, Lezcano-Gonzalez I, Peden CH, Szanyi J (2015) Chem Soc Rev 44:7371-7405.
2. Deka U, Lezcano-Gonzalez I, Weckhuysen BM, Beale AM (2013) ACS Catal 3:413-427.
3. Janssens TV, Falsig H, Lundegaard LF, Vennestrøm PN, Rasmussen SB, Moses PG, Giordanino F, Borfecchia E, Lomachenko KA, Lamberti C (2015) ACS Catal 5:2832-2845.
4. Groothaert MH, Smeets PJ, Sels BF, Jacobs PA, Schoonheydt RA (2005) J Am Chem Soc 127:1394-1395.
5. Woertink JS, Smeets PJ, Groothaert MH, Vance MA, Sels BF, Schoonheydt RA, Solomon EI (2009) P Natl Acad Sci USA 106:18908-18913.
6. Alayon EMC, Nachtegaal M, Bodi A, van Bokhoven JA (2014) ACS Catal 4:16-22.
7. Grundner S, Markovits MA, Li G, Tromp M, Pidko EA, Hensen EJ, Jentys A, Sanchez-Sanchez M, Lercher JA (2015) Nat Commun 6:7546.
8. Tomkins P, Ranocchiari M, van Bokhoven JA (2017) Acc Chem Res 50:418-425.
9. Sushkevich VL, Palagin D, Ranocchiari M, van Bokhoven JA (2017) Science 356:523-527.
10. Narsimhan K, Iyoki K, Dinh K, Román-Leshkov Y (2016) ACS Cent Sci 2:424-429.
11. Kulkarni AR, Zhao Z-J, Siahrostami S, Nørskov JK, Studt F (2016) ACS Catal 6:6531-6536.
12. Wulfers MJ, Teketel S, Ipek B, Lobo RF (2015) Chem Commun 51:4447-4450.
13. Saha D, Grappe HA, Chakraborty A, Orkoulas G (2016) Chem Rev 116:11436-11499.
14. Lunsford JH (2000) Cat Today 63:165-174.
15. Fickel DW, Lobo RF (2009) J Phys Chem C 114:1633-1640.
16. Deka U, Juhin Al, Eilertsen EA, Emerich H, Green MA, Korhonen ST, Weckhuysen BM, Beale AM (2012) J Phys Chem C 116:4809-4818.
17. Korhonen ST, Fickel DW, Lobo RF, Weckhuysen BM, Beale AM (2011) Chem Commun 47:800-802.
18. Borfecchia E, Lomachenko K, Giordanino F, Falsig H, Beato P, Soldatov A, Bordiga S, Lamberti C (2015) Chem Sci 6:548-563.
19. Andersen CW, Borfecchia E, Bremholm M, Jørgensen M, Vennestrøm P, Lamberti C, Lundegaard L, Iversen BB (2017) Angew Chem Int Edit 56:10367–10372.
20. Brandenberger S, Kröcher O, Tissler A, Althoff R (2008) Catal Rev 50:492-531.
21. Kwak JH, Zhu HY, Lee JH, Peden CHF, Szanyi J (2012) Chem Comm 48:4758-4760.
22. Gao F, Washton NM, Wang Y, Kollár M, Szanyi J, Peden CH (2015) J Catal 331:25-38.
23. Paolucci C, Parekh AA, Khurana I, Di Iorio JR, Li H, Albarracin Caballero JD, Shih AJ, Anggara T, Delgass WN, Miller JT (2016) J Am Chem Soc 138:6028-6048.
24. Martini A, Borfecchia E, Lomachenko KA, Pankin IA, Negri C, Berlier G, Beato P, Falsig H, Bordiga S, Lamberti C (2017) Chem Sci 8:6836-6851.
25. Palomino GT, Fisicaro P, Bordiga S, Zecchina A, Giamello E, Lamberti C (2000) J Phys Chem B 104:4064-4073.
26. Llabrés i Xamena FX, Fisicaro P, Berlier G, Zecchina A, Palomino GT, Prestipino C, Bordiga S, Giamello E, Lamberti C (2003) J Phys Chem B 107:7036-7044.

27. Pappas DK, Borfecchia E, Dyballa M, Pankin IA, Lomachenko KA, Martini A, Signorile M, Teketel S, Arstad B, Berlier G, Lamberti C, Bordiga S, Olsbye U, Lillerud KP, Svelle S, Beato P (2017) J Am Chem Soc 139:14961–14975.
28. Ipek B, Wulfers MJ, Kim H, Göltl F, Hermans I, Smith JP, Booksh KS, Brown CM, Lobo RF (2017) ACS Catal 7:4291-4303.
29. Giordanino F, Borfecchia E, Lomachenko KA, Lazzarini A, Agostini G, Gallo E, Soldatov AV, Beato P, Bordiga S, Lamberti C (2014) J Phys Chem Lett 5:1552-1559.
30. Lezcano-Gonzalez I, Deka U, Arstad B, Van Yperen-De Deyne A, Hemelsoet K, Waroquier M, Van Speybroeck V, Weckhuysen BM, Beale AM (2014) Phys Chem Chem Phys 16:1639-1650.
31. Lomachenko KA, Borfecchia E, Negri C, Berlier G, Lamberti C, Beato P, Falsig H, Bordiga S (2016) J Am Chem Soc 138:12025-12028.
32. Gao F, Mei D, Wang Y, Szanyi J, Peden CHF (2017) J Am Chem Soc 139:4935–4942.
33. Paolucci C, Khurana I, Parekh AA, Li S, Shih AJ, Li H, Di Iorio JR, Albarracin-Caballero JD, Yezerets A, Miller JT, Delgass WN, Ribeiro FH, Schneider WF, Gounder R (2017) Science 357:898-903.
34. Rehr JJ, Ankudinov AL (2005) Coord Chem Rev 249:131-140.
35. Bordiga S, Groppo E, Agostini G, van Bokhoven JA, Lamberti C (2013) Chem Rev 113:1736-1850.
36. Guda SA, Guda AA, Soldatov MA, Lomachenko KA, Bugaev AL, Lamberti C, Gawelda W, Bressler C, Smolentsev G, Soldatov AV, Joly Y (2015) J Chem Theory Comput 11:4512-4521.
37. Joly I, Grenier S (2016) Theory of X-ray Absorption Near Edge Structure In: van Bokhoven JA, Lamberti C (eds) X-Ray Absorption and X-ray Emission Spectroscopy: Theory and Application. John Wiley & Sons, Chichester (UK), pp 73-98
38. Van Bokhoven JA, Lamberti C (2016) X-ray absorption and X-ray emission spectroscopy: theory and applications, vol 1. John Wiley & Sons,
39. Garino C, Borfecchia E, Gobetto R, Salassa L, van Bokhoven JA, Lamberti C (2014) Coord Chem Rev 277–278 130-186.
40. Glatzel P, Bergmann U (2005) Coord Chem Rev 249:65-95.
41. Singh J, Lamberti C, van Bokhoven JA (2010) Chem Soc Rev 39:4754-4766.
42. Sano M, Komorita S, Yamatera H (1992) Inorg Chem 31:459-463.
43. Kau LS, Spirasolomon DJ, Pennerhahn JE, Hodgson KO, Solomon EI (1987) J Am Chem Soc 109:6433-6442.
44. Malinowski ER (2002) Factor analysis in chemistry. Wiley,
45. Tauler R (1995) Chemometrics Intell Lab Syst 30:133-146.
46. de Juan A, Tauler R (2003) Anal Chim Acta 500:195-210.
47. Elbergali A, Nygren J, Kubista M (1999) Anal Chim Acta 379:143-158.
48. Jaumot J, Gargallo R, de Juan A, Tauler R (2005) Chemometr Intell Lab 76:101-110.
49. Jaumot J, de Juan A, Tauler R (2015) Chemometr Intell Lab 140:1-12.
50. Conti P, Zamponi S, Giorgetti M, Berrettoni M, Smyrl WH (2010) Anal Chem 82:3629-3635.
51. Caetano BL, Briois V, Pulcinelli SH, Meneau F, Santilli CV (2017) J Phys Chem C 121:886-895.
52. Carvalho HWP, Pulcinelli SH, Santilli CV, Leroux F, Meneau F, Briois V (2013) Chem Mat 25:2855-2867.
53. Cassinelli WH, Martins L, Passos AR, Pulcinelli SH, Santilli CV, Rochet A, Briois V (2014) Catal Today 229:114-122.
54. Voronov A, Urakawa A, Beek Wv, Tsakoumis NE, Emerich H, Rønning M (2014) Anal Chim Acta 840:20-27.
55. Hong JP, Marceau E, Khodakov AY, Gaberova L, Griboval-Constant A, Girardon JS, La Fontaine C, Briois V (2015) ACS Catal 5:1273-1282.
56. Rochet A, Baubet B, Moizan V, Devers E, Hugon A, Pichon C, Payen E, Briois V (2017) J Phys Chem C 121:18544-18556.
57. Pascarelli S, Mathon O, Mairs T, Kantor I, Agostini G, Strohm C, Pasternak S, Perrin F, Berruyer G, Chappelet P, Clavel C, Dominguez MC (2016) J Synchrotron Radiat 23:353-368.
58. Ruckebusch C (2016) Resolving Spectral Mixtures: With Applications from Ultrafast Time-Resolved Spectroscopy to Super-Resolution Imaging, vol 30. Elsevier,
59. Ruckebusch C, Blanchet L (2013) Anal Chim Acta 765:28-36.
60. Mendieta J, Díaz-Cruz M, Esteban M, Tauler R (1998) Biophys J 74:2876-2888.
61. Bro R, De Jong S (1997) J Chemometr 11:393-401.
62. Bellet D, Gorges B, Dallery A, Bernard P, Pereiro E, Baruchel J (2003) J Appl Crystallogr 36:366-367.
63. Ravel B, Newville M (2005) J Synchrotron Radiat 12:537-541.
64. Godiksen A, Stappen FN, Vennestrom PNR, Giordanino F, Rasmussen SB, Lundegaard LF, Mossin S (2014) J Phys Chem C 118:23126-23138.
65. Gao F, Walter ED, Kollar M, Wang YL, Szanyi J, Peden CHF (2014) J Catal 319:1-14.
66. Godiksen A, Vennestrom P, Rasmussen S, Mossin S (2017) Top Catal 60:13-29.
67. Godiksen A, Isaksen OL, Rasmussen SB, Vennestrom PNR, Mossin S (2018) ChemCatChem 10:366-370.

68. McEwen J-S, Anggara T, Schneider W, Kispersky V, Miller J, Delgass W, Ribeiro F (2012) Catal Today 184:129-144.
69. Giordanino F, Vennestrom PNR, Lundegaard LF, Stappen FN, Mossin SL, Beato P, Bordiga S, Lamberti C (2013) Dalton Trans 42:12741-12761.